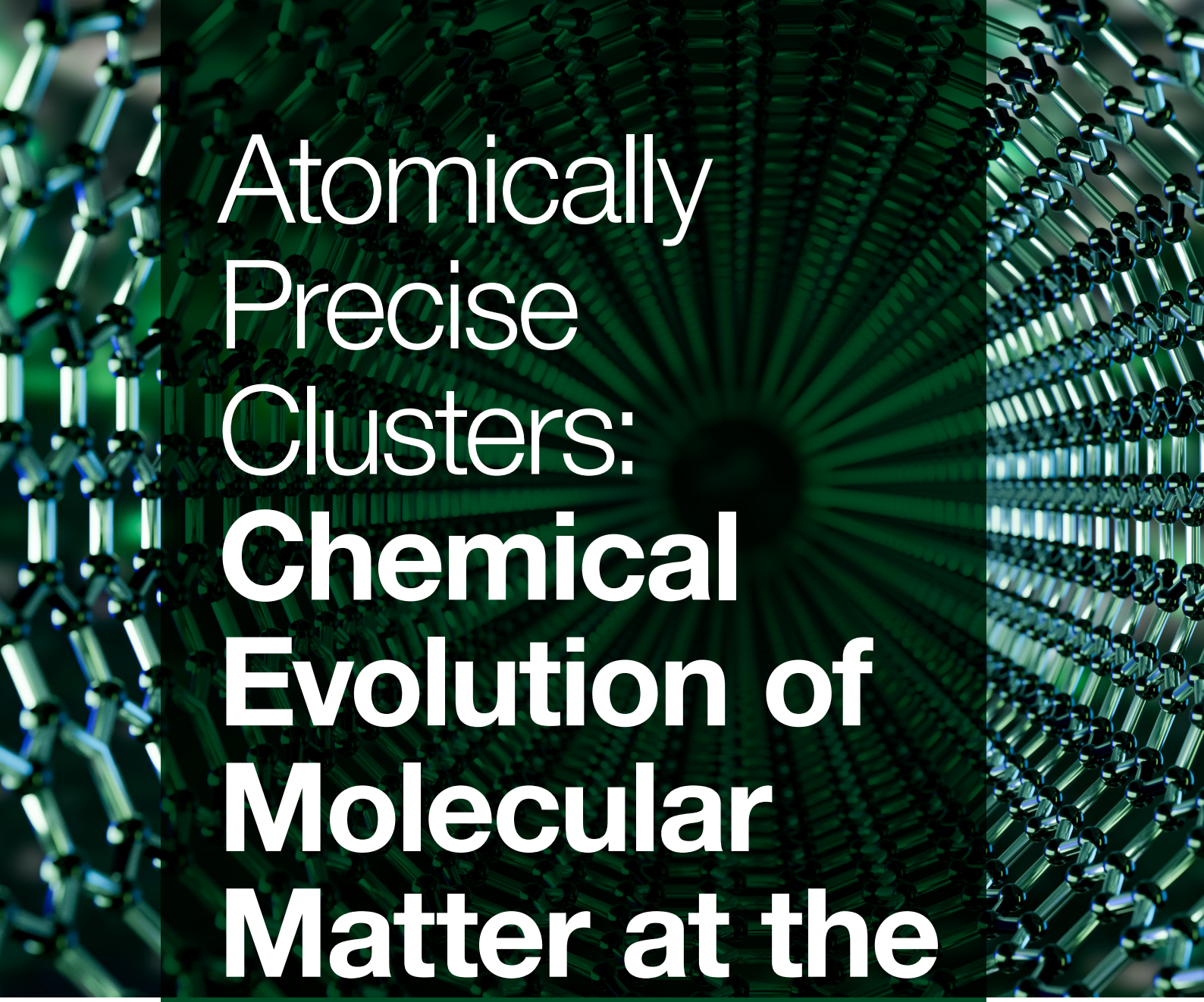

Atomically Precise Clusters: Chemical Evolution of Molecular Matter at the Nanoscale

by Arijit Jana, Amoghavarsha Ramachandra Kini, and Thalappil Pradeep

https://doi.org/10.51167/acm00040

The chemistry of nanoparticles with atomic precision has become a subject of interest due to the unique physical and chemical properties of these systems in comparison to their bulk counterparts. Nanoparticles typically contain thousands of atoms, arranged in a specific fashion. There is a need to bridge the gap between single atoms and nanoparticles to understand the size evolution of matter. This regime, composed of a few atoms, is called nanoclusters having size in the range of 1 to 3 nm, with a precise number of atoms, with well-defined structure and properties. Most of studied materials in this class are composed of noble metals. Various techniques, including UV/vis spectroscopy, mass spectrometry, and single crystal XRD, reveal their molecular nature. Their unique electronic properties can be used for applications in the fields of catalysis, sensing, magnetism, medicinal, bio-imaging, etc. This article touches upon the basics of nanoclusters, their synthesis, characterization, atomic structures, and supramolecular arrangements. We hope that this work provides a brief understanding of nanoclusters and inspires young scientists to conduct research in the chemistry of clusters.

Introduction to nanoclusters

There's plenty of room at the bottom,
Prof. Richard Feynman

Size-selected particles containing metal atoms are gaining increasing interest both in fundamental science and applications due to their tunable electronic structures and associated atom-specific functional properties. Traditional nanoparticles of metals with the dimension of 5-100 nm have continuous energy bands due to the overlap of valance and conduction bands. They exhibit surface plasmon resonance (SPR) features, in the absorption spectrum due to the oscillation of a large number of conduction band electrons. On the other hand, particles with dimensions <3 nm exhibit discrete electronic energy levels and manifest molecule-like multiple absorption features (Figure 1a, b). Other chemical properties of such ultrasmall particles depend on the shape, size, and composition of the particles. Even a single atom alteration can have a drastic effect on their physiochemical properties. Such ultrasmall particles with atomic precision are denoted by various names such as nanoclusters, clusters, aspicules, or nanomolecules. There are a number of review articles in the literature to know more about these systems.[1-3]

The synthesis of monolayer-protected nanoclusters mostly relies on metal thiolate reduction in a mixed solvent using suitable reducing agents, such as sodium borohydride, sodium cyanoborohydride, tertbutyl ammonium borane complex, hydrazine, etc.[4] A controlled synthetic conditions with specific temperature, pressure, solvent system and speed of stirring are involved in regulating the nuclearity of the cluster. Sometimes post-synthetic phase stability through excess ligand etching, thermal treatment, and size-focusing methods are used to convert polydispersed mixtures to monodispersed particles. The resulting samples show molecule-like characteristic optical signatures and undergo inter-cluster reactions like molecules, resulting in product nanoclusters. Ligand-exchange induced structural transformation (LEIST) is another synthetic method used for converting one cluster to another using excess ligands.[5,6] In general, phosphine and hydride-protected labile clusters are converted to thiolated clusters with higher thermodynamic stability. A few other methods, such as solid-state synthesis, photo reduction, microwave-assisted synthesis, hydrothermal and radiolytic reductions, were used to synthesize different nanoclusters.[1,2,4]

Transmission electron microscopic (TEM) investigations were performed to understand the atomic structure of such particles. Early TEM investigations of clusters revealed the presence of transient metal aggregates surrounded by an amorphous layer of ligands. Structural fluctuations of the ultrasmall metal core under the electron beam limits the quality of image acquisition. However, using a low-dose electron beam, measurement at cryogenic conditions, and advanced instrumentation resulted in good atomic imaging of a few nanoclusters. Palmer et al. observed rapid fluctuation of low symmetric chiral isomers of Au_{55} nanoclusters through time-lapse sequences of images collected using aberration-corrected scanning-TEM (STEM) (Figure 1c).[7] Recently, we have developed a methodology for atomic-scale imaging of crushed crystals of Ag_{25} and Ag_{29} clusters using a conventional transmission electron microscope at room temperature.[8] TEM micrographs show a layer-by-layer assembly of Ag_{29} clusters having an interlayer distance of 1.71, 1.97, and 2.42 nm, corresponding to (200), (111), and (110) lattice planes, respectively. Such a methodology can be extended for the structural investigation of unknown clusters.

Mass spectrometry (MS) is one of the principal techniques used to characterize nanoclusters. Two soft ionization techniques, electrospray ionization (ESI) and matrix-assisted laser desorption ionization (MALDI) were used to detect such molecular species in the gas phase. The negative ion-mode ESI-MS spectrum of a well-known cluster, i.e., Ag_{29} is presented in Figure 1e.[9] The isotopic purity of the cluster was understood by matching the experimental spectrum with the theoretical one. Along with the characteristic MS pattern, various other studies, such as collision-energy dependent fragmentation, ion-mobility separation, collision induced dissociation (CID) and surface-induced dissociation (SID), provides additional insight into their atomic structure. Intercluster reaction in solution resulted in new alloy clusters through the exchange of metal atoms, which was monitored through mass spectrometric studies.[10-12] Dynamic nature of the surface ligand promotes the exchange reaction, and new clusters were formed with mixed ligands. Theoretical investigations of intercluster reaction concluded that adduct dimeric species were formed in the intermediate step. Exact kinetic modeling of such reactions reveal such reactions occurs in three steps, a) formation of a dimeric species through interparticle interactions, b) atom exchange in dimeric species, and c) dissociation of dimers.[13] Kinetic simulation shows consecutive reactions starting from mother species which resulted in higher-order heterometal-doped sister species. Time-dependent ion intensities of the newly formed species measured through MS correlate well with kinetic modeling. The intercluster reactions between bimetallic and monometallic clusters leading to trimetallic clusters were also monitored through time-dependent MS studies.[14] Exchange of inner kernel metal atoms of the cluster by keeping the structure intact was first observed through MS studies.[15] Interparticle reactions between isotopically labeled $[Ag_{25}(SR)_{18}]$ clusters i.e., $^{107}Ag_{25}(SR)_{18}$ and $^{109}Ag_{25}(SR)_{18}$, show a rapid exchange of silver isotopes upon forming a transient dimer species.

The separation of isomeric clusters and their supramolecular adducts were also executed through ion-mobility MS studies. Isomers of glutathione-protected Ag_{11} cluster were distinguished in the gas phase as they have varying drift times in the ion mobility cell.[16] Combined CID and SID studies of such isomers show different fragmentation patterns, which suggested the existence of structural isomers. Another study demonstrated the formation of

Arijit Jana

Arijit Jana received his B.Sc. in Chemistry from the Ramakrishna Mission Vidyamandira and M.Sc. from IIT Madras. He is currently a PhD student at IIT Madras under Prof. Thalappil Pradeep. His research interests are on atomically precise metal nanoclusters, cluster-assembled framework solids and ambient electrospray deposition.

Amoghavarsha Ramachandra Kini

Amoghavarsha completed his B.Sc. and M.Sc. degrees in Chemistry from the University of Mysore. He is currently a PhD student at IIT Madras under Prof. Thalappil Pradeep. His research focus is on multimetallic alloy nanoclusters.

Thalappil Pradeep

Thalappil Pradeep is Institute professor and Deepak Parekh Institute chair professor in the Department of Chemistry at IIT Madras. He is also the professor-in-charge of the International Centre for Clean Water (ICCW). He earned his PhD degree from the Indian Institute of Science. Pradeep had post-docoral training at the University of California, Berkeley and Purdue University, West Lafayette. Major research fields in his group are in the areas of atomically precise nanoclusters, mass spectrometry, ice chemistry and water purification using nanotechnology.

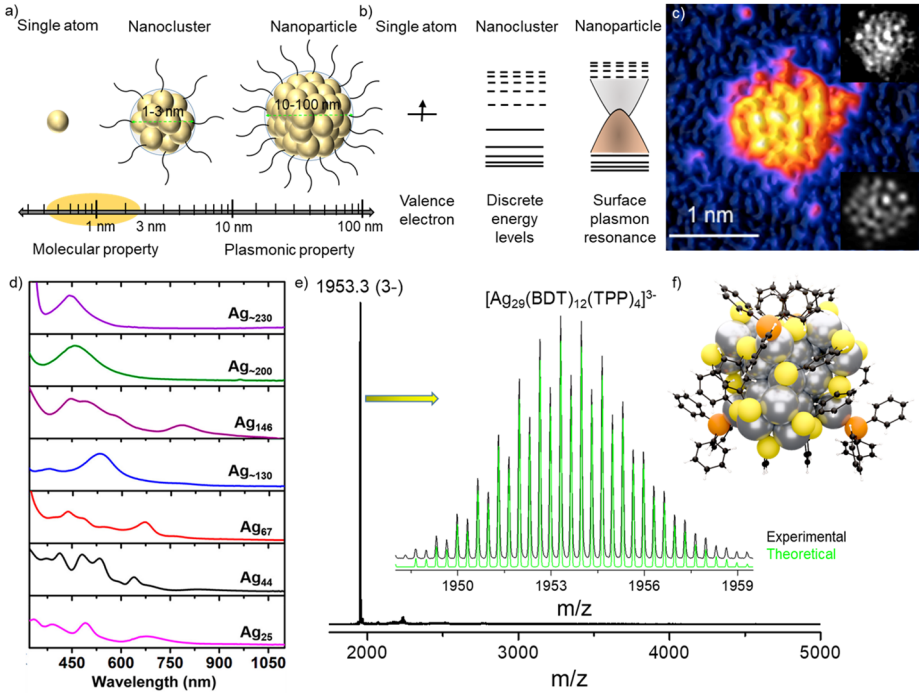

Figure 1: a) Schematic representation and b) energy level diagram of nanoclusters having a metal core protected by surface ligands and its comparison with nanoparticles. c) HAADF-STEM micrograph of Au_{55} nanocluster. Inset (top) real time frame and (down) simulated atomic imaging. d) Steady-state UV-vis absorption spectra of different silver nanoclusters with increasing nuclearity from the molecular to plasmonic regime. E) Full range mass spectrum of Ag_{29} in the negative ion mode. Inset shows the isotopically resolved experimental and simulated spectra. f) Atomic structural model of the same cluster. Reproduced with permission from Ref [7, 9, 37]

supramolecular adduct of cluster-fullerene aggregate promoted by weak intermolecular π-π, and CH-π interactions.[17] The MS spectrum shows the formation of hybrid species with a varying number of fullerene attachments with $Ag_{29}(BDT)_{12}$ cluster (where, BDT = 1,3 benzene dithiol). Furthermore, CID fragmentation studies of mass-selected adduct species reveal systematic detachments of fullerene moieties from the cluster. Host-guest complexation between the Ag_{29} cluster with cyclodextrins shows cis-trans isomerization of cyclodextrins over the surface of the cluster.[18] Different collision cross section (CCS) values of these isotopologues imply such isomerization promoted by weak intermolecular interactions. The symmetry of the cluster bonded with active surface ligands and the chemical nature of the guest species regulate the nature of these supramolecular isomers.

Atomistic understanding of structure

Single crystal x-ray diffraction (SC-XRD) studies successfully resolved the atomic structure of such materials. Single crystals are grown from a supersaturated solutions using antisolvent layering or vapor diffusion techniques.[19] Electrocrystallization of Au_{25} cluster using a small applied potential resulted in large-sized uniform crystals.[20] Till date, ~500 gold and silver clusters with various nuclearity were structurally understood through SC-XRD. In 2007, Kornberg et al. solved the first gold nanocluster, i.e., Au_{102} protected by 44 para-marcaptobenzoic acid ligands, at a resolution of 1 Å.[21] This nanocluster has 49 atoms with a decahedron inner core having an Au-Au distance of 2.8-3.1 Å, clasped with extra gold atoms in an unanticipated fashion. Later, several nanoclusters were structurally resolved through single-crystal XRD. In general, the atomic arrangement was illustrated to be composed of an inner layer of metal atoms, called an inner kernel/core, enclosed by an outer layer of metal atoms, further protected by ligands. The inner kernel with tetrahedral (Td), octahedral (Oh), cubic, icosahedral, square antiprismatic, and distorted structures were observed for various gold and silver nanoclusters. The outer layer remains open or becomes distorted for some clusters due to steric accommodation of ligands, metal-ligand interfacial movement, and binding stability of metal atoms. Electron diffraction of the microcrystalline sample is also used to structurally determine such atomically defined particles. Azubel et al. resolved the atomic structure of the Au_{68} cluster using a low-dose aberration-corrected transmission electron microscope.[22] Recently, neutron diffraction and scattering studies were performed to resolve the atomic structure with a satisfactory resolution.[23] Especially the position of atoms with less electron density, such as hydrides, sulfides, carbides, and chlorides is precisely located using this technique. Deep learning coupled with various diffraction methods is also involved in structure determination in the field.[24]

> ***'Each of us have things and thoughts and descriptions of an amazing universe in our possession that kings in the 17th century would have gone to war to possess'***
> Prof. Kary Mullis

Several nanoclusters were reported to have fused inner kernel structures. The fusion of icosahedral (M_{12}) or central-icosahedral (M_{13}) units through the vertex, edge, and face-sharing modes create di, tri, tetra, and pentameric series. In 2007, Shichibu et al. synthesized an Au_{25} nanocluster protected by n-alkane thiol, formed by the fusion of two icosahedral units by sharing one vertex.[25] This nanocluster looks like a rod-shaped molecule, contrary to the well-known structure of Au_{25}, which has a central icosahedral core surrounded by six Au_2SR_3 surface staples arranged in an octahedral fashion. This structure extends to three icosahedral units arranged in a straight line forming a linear tri-icosahedral unit with 37 gold atoms.[26] The optical absorption spectra show a gradual reduction of the band gap of 1.96, 1.73, and 0.83 eV for Au_{13}, Au_{25}, and Au_{37}, respectively, which suggest constant evolution of energy levels upon structural fusion of icosahedral units. Last year, Wang et al. synthesized a rod-shaped silver nanocluster, i.e., Ag_{61} having four icosahedral units connected linearly through vertex sharing.[27] UV-vis spectrum shows a strong absorption peak at the near-infrared region due to one-dimensional electronic coupling between the icosahedral units.

The fusion of cores through vertex sharing gives beautiful structures evident from the cyclic arrangement of three icosahedral units in $M_{37/38}$ (M= Au/Ag, an alloy nanocluster with the formula $Au_{18}Ag_{19/20}$) has a cyclic arrangement of five Au_{13} through vertex sharing. The fusion of the icosahedral core can also happen through face sharing, as reported for the Au_{38} nanocluster. This cluster has bi-icosahedral Au_{23} cores fused through a triangular face. The fusion of cores through edge-sharing was theoretically investigated by Hakkinen et al. for several nanoclusters, including $Au_{40}(SH)_{24}$, $Au_{57}(SH)_{32}$, $Au_{74}(SH)_{40}$, and $Au_{108}(SH)_{56}$.[29] Here, the icosahedral cores share an edge with a 90° rotation

from each other. Using the theoretical models set for clusters mentioned above, they could predict the structure of a new cluster, $Au_{54}(SR)_{30}$.[30]

The tetrahedral core consists of four metal atoms that show interesting fused arrangements for a higher-order assembled kernel. Zeng et al. reported the double-stranded growth of tetrahedral cores in a series of clusters with a general formula of $Au_{8n+4}(TBBT)_{4n+8}$ (with n ranging from 2 to 6 and TBBT is 4-tert-butylbenzenethiolate ligand). The clusters they reported are $Au_{20}(TBBT)_{16}$, $Au_{28}(TBBT)_{20}$, $Au_{36}(TBBT)_{24}$, $Au_{44}(TBBT)_{28}$, and $Au_{52}(TBBT)_{32}$, having 2, 4, 6, 8, and 10 tetrahedral units, respectively.[31] The Au_{20} is formed by vertex sharing of two tetrahedra. This structure was extended to Au_{28} with two strands of vertex-sharing tetrahedra, each arranged in a double helical fashion. This structure extends in the same manner from Au_{28} to Au_{52} in two strands in a double helical manner, where Au_{52} contains two strands of five vertexes sharing an icosahedron each. Tetrahedral cores have also been reported to form cyclic arrangements in Au_{22}, Au_{28}, Au_{34}, and Au_{40} nanoclusters having 1, 2, 3, and 4 bi-tetrahedral units with 7 Au atoms, respectively. The cubic core has eight metal atoms fused in a series of clusters, i.e., Ag_{14}, Ag_{38}, and Ag_{63}, having 1, 4, and 8 fused cubes, respectively.

A handful of nanoclusters with large nuclearity, i.e., M_mL_n, m = 150-1000, were structurally resolved. A few examples are $[Au_{156}(C{\equiv}CR)_{60}]^{32}$, $[Au_{191}(SPh\text{-}^tBu)_{66}]_{30}^{33}$, $[Au_{246}(SR)_{80}]^{34}$, $[Ag_{307}Cl_{62}(SPh^tBu)_{110}]^{35}$ and $[Ag_{374}(SR)_{113}Br_2Cl_2]^{36}$. The structural anatomy of these clusters reveal that they have multilayered core-shell arrangements of metal atoms, and a ligand shell uniformly protects the outer layer. For example, Au_{156} has a concentric Au_{126} core composed of Au_{46}-Au_{50}-Au_{30} layered geometry having length and width of 2.38 and 2.04 nm, respectively. The unidirectional Au_{46} inner kernel is composed of one icosahedron (Au_{12}), two fused flattened icosahedra (Au_{11}), and two terminal pentagonal pyramids (Au_6) connected in a linear fashion. The Au_{46} inner kernel is further protected by a drum-like Au_{50} tube and covered by a belt-shaped third shell of 30 gold atoms. The outermost shell consists of 30 gold atoms connected with 60 alkynyl ligands. UV-vis absorption spectrum of these clusters exhibits a single plasmonic absorption feature centered at ~ 500 nm. A series of silver nanoclusters, having 25, 44, 67, 130,146, 200, and 230 atoms, manifest such variation of ground state absorption features upon gradually increasing atomicity (Figure 1d).[37] These large clusters are the missing link between molecular and metallic nanoparticles.

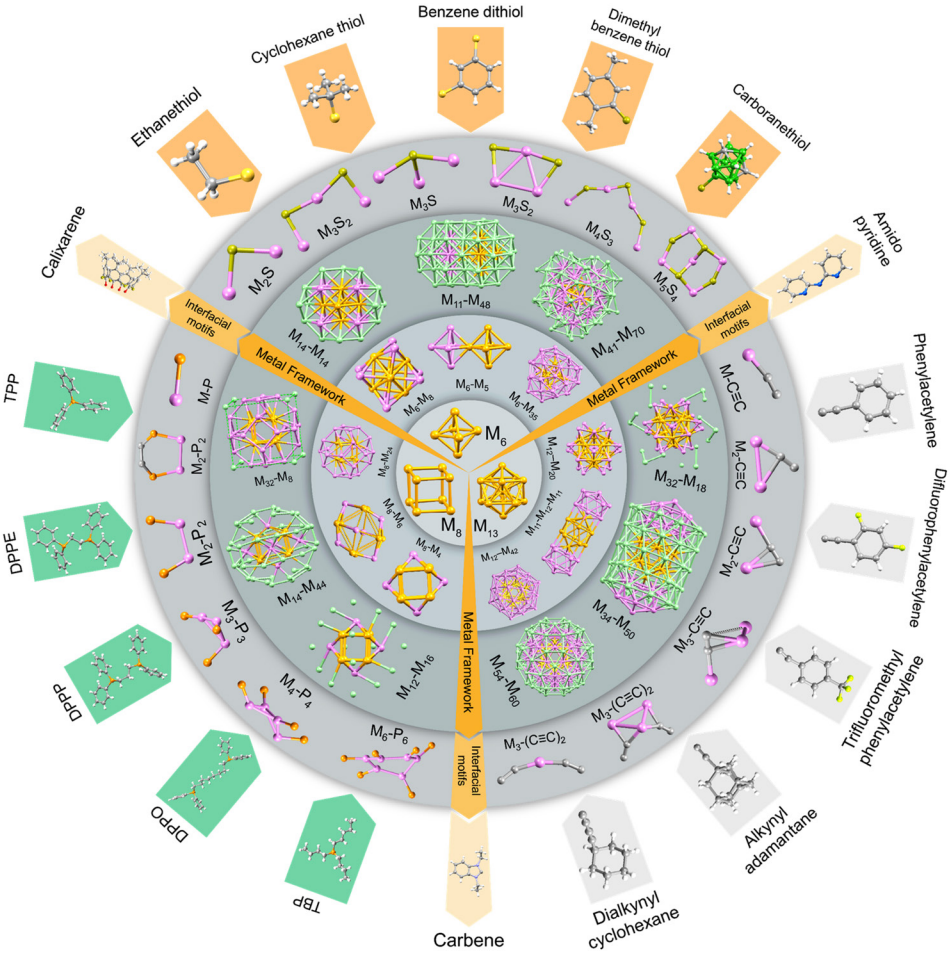

Figure 2: Illustration of the structural model of monolayer protected metal nanoclusters having different types of multilayered core-shell geometry, interfacial motifs and surface ligands. Reproduced with permission from Ref [27, 32, 46, 50, 51, 65]

Ligands play an essential role, not just by shielding the metal core but also they determine the chemical properties of the cluster. The instability of bare clusters due to their excessive surface reactivity limits their study in the condensed phases. They have been synthesized in the gas phase under ultrahigh vacuum, and various properties of bare clusters were studied in the same condition. The ligands, i.e., thiols, phosphines, alkynes, carbenes, calixarene, and amido-pyridines are used for synthesizing metal clusters.[1-3] For thiol-based ligands, different metal-sulfide linkages bridge the metal core and peripheral ligands. A few such staple motifs are a) monomeric (–M-S-M-, -M_3-S), b) dimeric (-M-S-M-S-M-), c) trimeric (-M-S-M-S-M-S-M-) and d) tetrameric (M_5S_4) units present for a thiolated metal cluster. Positional isomerism of the thiol group present in the ligand can regulate the nuclearity of nanoclusters. Chen et al. observed size tuning of gold clusters from Au_{130}(p-MBT)$_{50}$, Au_{104}(m-MBT)$_{41}$, to Au_{40}(o-MBT)24 (where MBT is methylbenzene thiol) upon changing the ligand from para, meta to ortho-MBT.[38] This type of decreasing trend in atomicity is due to the increasing steric hindrance of the secondary methyl group in the ligands. The binding of phosphine ligands through metal-phosphine bonds also resulted in clusters. Sometimes phosphine ligands act as secondary ligands weakly bonded with the outer cluster shell. Alkyne ligands are bonded with the cluster through C≡C end through linear, L and V-shaped staple motifs via σ and π-bonding. Electronic distribution through π-conjugation results in different absorption, emission and catalytic activity of alkynyl protected nanoclusters. Figure 2 summarizes different types of kernel structure, interfacial motifs and ligand shell present in clusters.

Intercluster assembly

Understanding the supramolecular assembly of clusters within a single crystal is important to correlate their various solid-state properties, such as conductivity, luminescence, chirality, mechanical, and catalytic properties. Generally, clusters are packed in a layer-by-layer (AB···AB, ABC···ABC) fashion in the lattice. For example, the crystal has a well-known Au_{25} cluster-packed a face center cubic (fcc) structure.[39] On the other hand, the silver analogue, Ag_{25} is packed in a AB···AB mode along the b and c axis.[40] A recent report by Jin et al. demonstrated

DNA helix-like packing of heterodimeric $Au_{29}(SAdm)_{18}$ nanocluster (where SAdm = Adamentane thiolate).[41] Structural fusion of two clusters i.e., $Au_{30}(SR)_{18}$ and $Au_{28}(SR)_{20}$ resulted in such heterodimeric nature. Anisotropic interactions between two enantiomers through specific pairs of ligands contributed to this double helical assembly. Higher-order tetra helical arrangement was also observed.

Just as organic molecules and other natural objects, nanoclusters act as chiral atomic entities. The chirality of such nanomaterials originates due to a) chiral ligand, b) helical staple motifs, c) chiral kernel structure, and d) intercluster packing. Generally, the outer ligand shell induces chirality to the core metal atoms.[42] Separating optically pure isomers of individual nanoclusters from the solution is challenging due to their sizeable macromolecular structure and rapid interconversion rate. Sun et al. demonstrated spontaneous resolution of racemic Ag_{14} clusters through re-crystallization in acetonitrile solvent.[43] Homocluster crystallization is favored through hydrogen bonding interactions between surface ligands and solvent molecules. Another report by Mak et al. shows enantiomeric self-assembly of Ag_{30} upon re-crystallization in dimethyl acetamide (DMAC) solvent.[44] Chirality of the nanocluster arises from the spiral arrangement of the ligands directed by unusual B–H···π and C–H···π bonding interactions among the carborane cages and the benzene rings. Noncovalent weak interactions of DMAC with the ligand shell of the clusters favor crystallization of R and L-isomers together. The use of external chiral ligands sometime helps to crystallize specific isomers. Nakashima et al. separated chiral isomers of $[Ag_{29}(BDT)_{12}(TPP)_4]$ nanocluster using a chiral high-performance liquid chromatography (HPLC) column.[45] Separated isomers show mirror image circular dichroism (CD) spectra, which imply their optical purity. Theoretical calculations reveal chiral column helps the chirality induction of Ag_{29} through the interactions with the outer interior of staple motifs. Another report from our group showed a propeller-shaped structure with six rotary arms in a Ag_{21} nanocluster, primarily protected by meta-carborane 9-thiol ligands.[46] The staggered arrangements of six peripheral carboranes determine the rotary nature of the cluster. Therefore, efficient tuning of the ligand shell will result in various structural frameworks.

Sometimes two or more different ways of intercluster packing were observed for a particular cluster, known as polymorphism. We have observed polymorphism on Ag_{29} nanocluster with cubic and trigonal crystal systems.[47] Crystallization of the cluster in the DMF solution through the slow evaporation method generates cubic crystals. In contrast, vapour diffusion of methanol into the DMF solution resulted in trigonal crystals (shown in Figure 3). The stronger CH···π and H···H van der Waals interactions between the secondary triphenylphosphine ligands resulted in the cubic form compared to the trigonal system. Both crystals look similar to the naked eye, however rigidity of cubic crystals augmented stronger luminescence compared to trigonal crystals. Another report shows ligand-induced isomorphism of $Au_{28}(SR)_{20}$ nanoclusters protected by cyclohexyl-thiol (CHT) and 4-tert-butylphenyl thiol (TBPT), respectively.[48] Despite having similar inner kernel structures, the outer $Au_8(SR)_{12}$ staples are arranged in two trimeric and two monomeric units for Au_{28}@CHT, whereas through four dimeric units for the Au_{28}@TBPT cluster. Such variation of the outer shell induced isomerization of the cluster influenced their catalytic activities.

A single crystal grown by a purified nanocluster leads to the assembly of specific particles in the lattice. In some cases, solvent molecules or counter ions were crystallized along with the nanocluster. Cocrystals are formed by crystallizing two clusters inside the unit cell through favorable intermolecular interactions.[49] In 2018, Zheng et al. prepared the first thiolate-protected cocrystal, i.e., $(AuAg)_{45}(SR)_{27}(PPh_3)_6$ and $(AuAg)_{267}(SR)_{80}$ by the reduction of metal thiolate.[50] The trigonal prismatic smaller $(AuAg)_{45}$ cluster (particle dimension of 1.1 nm) is packed with the spherical larger cluster having a particle dimension of 2.5 nm. These diversified particles, in terms of their shape and size packed themselves in the crystal through ligand-centred CH···π interactions. Supramolecular packing of the cocrystal demonstrated a hexagonal arrangement of each particle. We synthesized dimethyl benzene thiol (DMBT) and triphenylphosphine-protected Ag_{40} and Ag_{46} cocrystals with the same outer shell but different inner core structures.[51] During crystallization, these particles were not distinguishable due to the identical arrangement of the outer shell i.e., $[Ag_{32}(DMBT)_{24}(TPP)_8]$. Mass spectrometric studies of a few such crystals dissolved in suitable solvents further verified the presence of both these clusters in the crystal. Another report from our group showed the intercluster reaction between triphenylphosphine and hydride-protected Ag_{18} and tert-butylthiol (TBT) protected Ag_{12} nanoclusters resulting in Ag_{16} and Ag_{17} clusters, primarily protected by TBT ligands. Subsequent crystallization of as-synthesized clusters resulted in a cocrystal of Ag_{16}:Ag_{17} having 2:1 occupancies in the crystal.[52] The indistinguishable metal-chalcogenolate outer shell having an $Ag_{16}S_8$ unit possess simultaneous crystallization of the clusters. Until now, ~10 cocrystals have been structurally resolved using X-ray crystallography.[53,54]

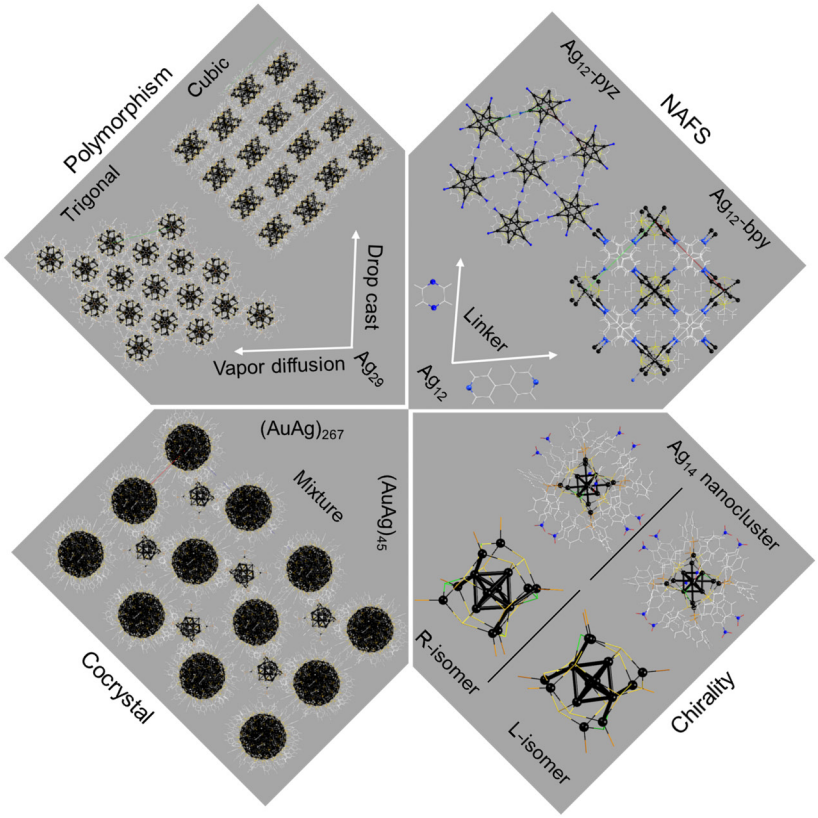

Figure 3: Structural representation of intercluster packing resulted polymorphic crystals, cocrystals, chirality and nanocluster assembled framework solids. Reproduced with permission from Ref [43, 47, 50, 57]

Assembly of nanoclusters using suitable organic linkers forms a porous framework structure, known as nanocluster assembled framework solid (NAFS). They are structurally similar to traditional metal-organic frameworks (MOFs). Instead of a single metal atom as a node for MOFs, a cluster core of aggregated metal atoms act as a node for such materials. Multidentate N-donor ligands, such as bipyridine (bpy), pyrazine (pyz), 1,2-bis(4-pyridyl)ethane (bpe), 1,2-di(pyridine-4-yl)diazene (dpd), tris(4-pyridylphenyl)-amine (tppa), 5,10,15,20-tetra(4-pyridyl) porphyrin (tpp), etc., are used as linkers for various NAFS. Such linkers promoted large-order intercluster assembly, which incorporates the stability of the framework and creates unique materials combining the optical and electronic properties of cluster and organic linkers. Mak et al. synthesized the first NAFS having an Ag_{12} cluster node interconnected by 4,4′-bpy linkers.[55] The resulting NAFS show superior stability for up to a year compared to clusters, which degraded within 30 min in ambient conditions. A structural framework having multiple nanochannels of these materials promotes the adoption of volatile organic molecules. Drastic variation of the electronic properties was observed in this NAFS compared to the bare cluster. Mak et al. demonstrated the site-specific assembly of superatomic Ag_{14} cluster through bidentate N-donor pyridyl ligands.[56] Eight open vertices of the cluster promote differently ordered assemblies. Steric availability of the ligands is the most influencing factor behind higher-ordered framework assembly. Another interesting NAFS, i.e., Ag_{12}-pyz reported from our group with pyz linkers, shows a distinct variation of the cluster structure compared to Ag_{12}-bpy through metal-metal and metal-sulfide rearrangements promoted by the linkers.[57] SCXRD reveals a graphene-like hexagonal layered assembly of the NAFS. Successful exfoliation of each layer from the parent crystals through ultra-sonication enables us to image each layer through transmission electron microscopy. Crosslinking between framework structures resulted in a hybrid flexible membrane as shown by Zang et al.[58] Accessible amino groups present in the linkers covalently crosslinked with acrylate monomers through photoinduced polymerization propagated along the membranes provided them with superior photoemission characteristics.

Emerging properties

Technology plays a key role in sustaining the modern world, and there is a continuous effort to make smaller devices for portability and versatility without compromising performance efficiency. Nanoclusters and their superstructural assembly have emerging potential with fascinating properties, such as luminescence, chiroptical behaviour, conductivity, photoconductivity, etc. Here, we provide a brief account of research towards studying various properties of nanoclusters in the past few years.

Photoluminescence:

Photoluminescence (PL) is an interesting property observed for several nanoclusters due to the radiative relaxation of the excited states between closely spaced electronic energy levels. PL properties have potential applications in the field of sensing, bioimaging, and optoelectronic devices.[1-3] Although most clusters are red emitting (depicted in Figure 4a), the emission wavelength of clusters usually varies from greenish-yellow (λ = 450 nm) to near-infrared (λ = 1500 nm) region. For example, ortho-carborane 1,2 dithiol protected Ag_{14} cluster has red luminescence centered at λ_{max} 626 nm using excitation at 370 and 450 nm (shown in Figure 4b). Generally, silver nanoclusters are better fluorophore than gold clusters in terms of emission brightness, quantum yield, colour tunability and photostability. The structural framework of the metal atoms, metal-ligand interface, electronic nature of the surface ligands and surrounding environment determines the emission characteristics of such materials.[59] Isomerization also have significant effect on PL properties. Jin et al. demonstrated that $Au_{28}(CHT)_{20}$ shows ~15-fold higher emission than $Au_{28}(TBBT)_{20}$, where CHT is cyclohexane thiol and TBBT is p-tert-butylbenzenethiol.[60] The absorption spectra of both these clusters are similar having a HOMO-LUMO gap of around 1.7 eV; however, PL emission properties are different. Despite having a similar Au_{14} kernel, the arrangement of the outer staple motifs determines the relaxation dynamics. Femtosecond transient absorption studies further reveals that surface staple motifs to kernel centre charge transfer is responsibe for such a behavior.

> ***The Science of today is the technology of tomorrow,***
> Prof. Edward Teller.

Sometimes aggregation resulted in enhanced emission of clusters, popularly known as aggregation-induced emission (AIE) or aggregation-induced enhanced emission (AIEE).[61] Zhu et al. observed 13 times bright emission (QY of 0.9 to 11.7%) of $[Ag_{29}(BDT)_{12}(TPP)_4]$ upon gradual addition of TPP ligands into the DMF solution of the cluster.[62] Restriction of the dynamic dissociation process of TPP ligands promotes PL enhancement by reducing the non-radiative transition processes. Mass spectrometric studies also verified such dynamic dissociation of the cluster. We have also observed similar luminescence phenomena of the same cluster by changing the secondary ligands from monophosphines to diphosphines.[63] Increasing the chain length of such bidentate ligands enhances the emission ~30-fold through a ligand-to-metal charge transfer (LMCT) mechanism. Crystallization is another type of aggregation that also results in enhanced emission. The first crystallization-induced emission enhancement (CIEE) behavior was observed in a bimetallic $[Au_4Ag_{13}(dppm)_3(SR)_9]$ nanocluster, which becomes strongly emitting upon forming crystals.[64] The cluster is non-emitting in solution and weakly emitting in amorphous conditions. Restriction of intramolecular motions in the crystalline state through C-H···π interaction enhances the radiative transition. We observed similar behavior in a silver cluster, i.e., $[Ag_{22}(2,5\text{-DMBT})_{12}(DPPE)_4Cl_4]^{2+}$ having a distorted Ag_{10} core protected by an Ag_{12} shell.[65] PL profile of CIE behavior is shown in Figure 4c. This superatomic cluster with four magic electrons promotes intermolecular interactions through short contact C-H···π, and π···π interactions which favor its CIE nature.

PL properties of the nanoclusters generally increase upon reducing the surrounding temperature. Restricting intramolecular motion in cryogenic conditions increases the excited state's radiative relaxation. Sun et al. observed similar phenomena of gradual increase of emission intensities of gold and silver nanoclusters, i.e., Au_8, Au_{13}, Ag_{44}, Ag_{50}, Ag_{64}, Ag_{73}, Ag_{80}, and Ag_{90}, upon reducing the temperature.[59] We have also observed a similar phenomenon of carborane-thiol protected Ag_{14} nanocluster (Figure 4d), which shows > 25-fold enhanced emission upon reducing the temperature from 298 to 77 K (Figure 4e).[66] The reduction of intensity might not always be linear with temperature. A large buckyball-type Ag_{180} cluster shows nonlinear PL enhancement upon reducing the temperature from 293 to 193 K in its crystalline state with 30 nm blue-shifting of emission maxima.[67] Further reducing the temperature from 193 to 93 K shows linear enhancement of emission intensity.

Gu et al. observed pressure-induced emission enhancement of gold nanoclusters by applying hydrostatic pressure through a diamond anvil cell (DAC) (shown in Figure 4f).[68] They have performed in situ optical spectroscopic measurements using $[Au_{21}(SR)_{12}(dppm)_2]^+$, and $[Au_{28}(SR)_{20}]$ having mono and bi cuboctahedral structure and $[Au_{24}(SR)_{20}]$ and $[Au_{14}Cd(SR)_{12}]$ having bi-tetrahedral metal kernel, respectively. Redshifting of the absorption spectra upon gradually increasing pressure was

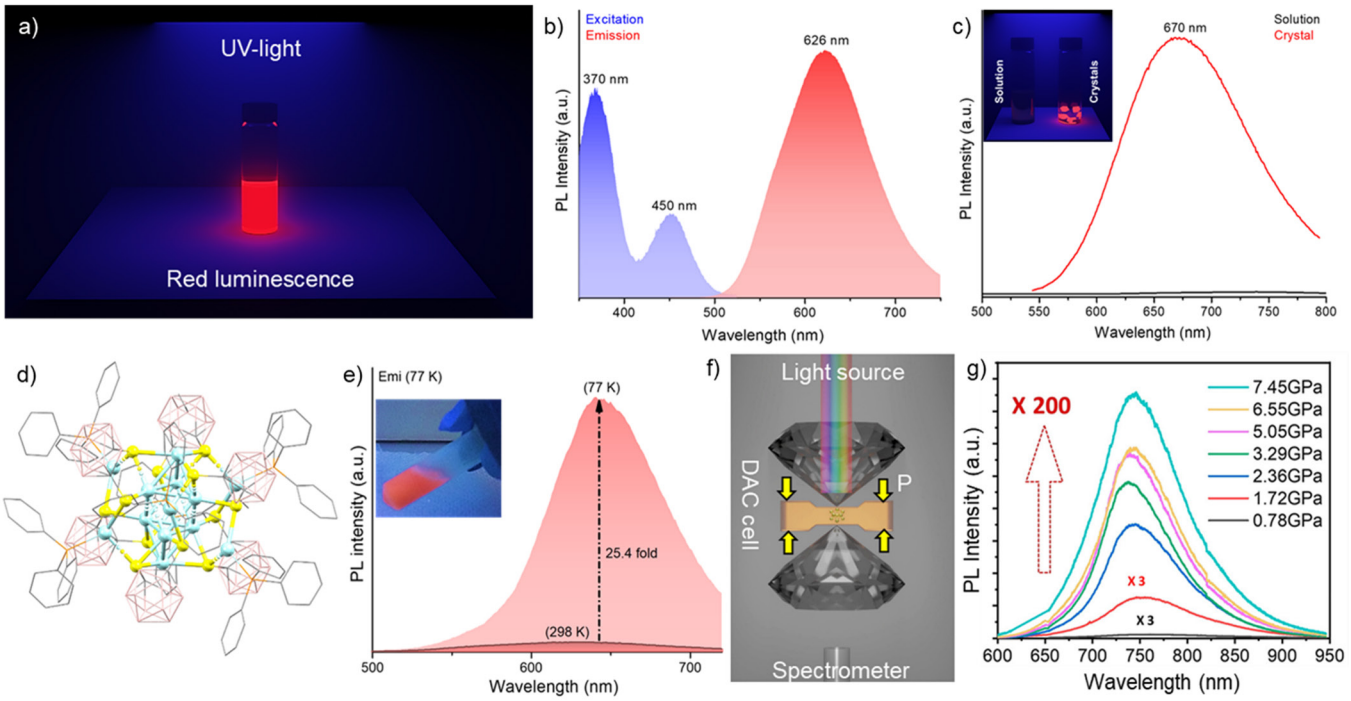

Figure 4: a) A schematic depiction of a nanocluster solution emiting red color under UV light. b) Excitation and emission spectral profile of a red emitting Ag_{14} nanocluster. c) Crystallization-induced-emission spectra of Ag_{22} nanocluster. Inset shows the illustration of of luminescence of solution at 77 K. and single crystals. d) Molecular structure of Ag_{14} nanocluster. e) Temperature-dependent PL profile of the same cluster (inset shows a photograph at 77 K). f) A schematic representation of DAC used for hydrostatic pressure-dependent optical measurements. g) Pressure-sequence PL spectra of $[Au_{14}Cd(SR)_{12}]$ cluster shows 200-fold emission enhancement. Reproduced with permission from Ref [65, 66, 68]

observed for all the clusters. DFT calculation shows induced electron delocalization over ligands upon squeezing the cluster, narrowing the spacing of energy levels. PL investigation reveals emission enhancement for all these clusters and ~200-fold highest emission enhancement at ~7 GPa for the $[Au_{14}Cd(SR)_{12}]$ cluster (Figure 4g). Such emission enhancement is due to the reduction of excited state structural distortion, which eventually enhances the near-band-edge transition dipole. Another report by Zang et al. displays the piezochromic behavior of Ag_{50} cluster crystals.[69] Reversible color tuning of the crystals from orange-red to dark red upon increasing the pressure from 1 atm to 7.5 GPa, correlated well with the reduction of the optical band gap.

NAFS also behave as tunable luminescence materials. The bare Ag_{12} nanocluster is red emitting (λmax = 620 nm), however, Ag_{12}@4,4′-bpy NAFS is green emitting (λmax = 507 nm) in its crystalline state.[55] A 60-fold enhancement of PL quantum yield (0.2 % to 12.1 %) upon forming a framework structure signifies the role of an ordered arrangement of chromophores. The emission colors of this NAFS was shifted from green to orange-yellow in the presence of volatile organic compounds (VOCs) such as ethanol, acetonitrile, chloroform, and 2-cyanoethanol, etc. The emission intensity of this material increases linearly upon increasing the vapor pressure of ethanol from 0 to 1.33 kPa, showing the linear response, which further implies the tangible incorporation of ethanol molecules in the cavity. The alteration of electronic structure upon encapsulation of such VOCs is due to the formation of inclusion complexes through π···π, and hydrogen bonding interactions with adjacent layers. Single crystals of such inclusion complexes further verified the inclusion of VOCs in the lattice. Ultrafast multicolor luminescence switching has enormous potential in optical sensors, luminescence signaling devices, and other optoelectronic applications.

Conductivity

Miniaturization of electronic devices has been evident recently due to the growth of single-atom transistors, memory devices, etc. Nanoclusters are a great option for making nanoscale conducting fibers, crystals, and other superstructures, which can be used for various nano-dimensional electronic applications like photoconductivity, sensors, field effect transistors (FETs), and many more. First, we will discuss the photoconductive behavior of a randomly assembled fibrous network of Ag_{88} nanocluster.[70] The comparative photoconductivity of two nearly isostructural Ag_{88} clusters i.e., Ag_{88}-A and Ag_{88}-B, primarily protected by thiacalixarene ligands. Authors have prepared a one-dimensional nanotubes to study their photoconductive behavior in electrochemical conditions (0.2 M aqueous Na_2SO_4) through a three-electrode setup. Linear sweep voltammetric (LSV) profile showed that Ag_{88}-B has a better photocurrent response (0.20 μA/cm^2) than the first one, having a photocurrent response of 0.12 μA/cm^2. Intercluster assembly reveals that Ag_{88}-A assembled in a face-to-face fashion, while Ag_{88}-B arranged as face-to-side through intercluster noncovalent interactions of tert-butyl groups. The structural asymmetry of the Ag_{88}-B cluster with specific packing promotes higher electron mobility than the other one.

Li et al. demonstrated the hierarchical assembly of Au_{21} nanoclusters in crystals by changing the counter ions (i.e., $AgCl_2^-$ and Cl^-) during crystallization.[71] The two counter ions reside near the diphenyl ligands through anion-π and aryl C-H···Cl interactions. The Au_{21} nanoclusters are assembled linearly along the diagonal of (100) and (010) planes for Au_{21}@$AgCl_2^-$ and Au_{21}@Cl^- clusters, respectively. The different crystal packing of the two Au_{21} nanoclusters and the different counterions resulted in a difference in the conductivity of these two clusters, which was measured and characterized by measuring the I-V curves for the clusters. The average electrical conductivity (σ) of Au_{21}@$AgCl_2^-$ was ~ 1.44×10^{-8} S/m and for Au_{21}@Cl^- it was ~ 2.38×10^{-6} S/m, averaged over 6 to 7 crystals. The conductivity in a material like a crystal or an assembly of nanoparticles depends on the interparticle distance, i.e., higher conductivity is observed at lower

interparticle distances (a general rule is that there will be ~1 order of magnitude change in conductivity for every 1 Å change in interparticle distance). The center-to-center distances between the adjacent clusters in crystals with $AgCl_2^-$ and Cl^- counterions are 16.80 and 16.39 Å, suggesting that the clusters are closer together in Au_{21}@Cl– and hence the conductivity of this cluster crystal should be higher than Au_{21}@$AgCl_2^-$ cluster, which is also supported by the σ values of the clusters. Here the interparticle distance differs only by a small magnitude, but the conductivity increases by two orders of magnitude; hence the interparticle distance cannot be the only factor affecting the change in conductivity of these clusters. Further studies are needed to understand the mechanism of electron transport through crystals.

Clusters can also be used for FET applications by transporting electricity along specific crystal axes. Yuan et al. demonstrated such a behavior of an alloy cluster with a composition of $Au_{21.3}Ag_{12.7}L_{20}$ (where L is 1-ethynyladamantane).[72] This cluster crystallizes in two forms depending on the solvent system. When the clusters are crystallized in the chloroform-methanol system, they form a monomeric unit, and when crystallized in the dichloromethane-methanol system, they form a one-dimensional polymer-like assembly into the crystal (shown in Figure 5a) through Ag–L–Au–L–Ag linkages. Authors have fabricated FET devices using Si wafers, coating them with 300 nm SiO_2 and depositing four terminal electrodes onto them. The crystals were painted at suitable positions with silver paste to create contacts with the electrodes. Using this device, they studied the one-directional conductivity through crystals along the a and c axis. Electrical conductivity was measured by the slope of the linear I-V curve along the a and c-axis, as shown in Figure 5b. The crystal's conductivity along the c-axis was found to be 1.49 × 10^{-5} Sm^{-1} which is 1800 times more than the conductivity along the a-axis (shown in Figure 5c). In the crystal, there is anisotropy, where the clusters are connected along the c-axis but are not in contact and insulated by the bulky adamantane ligands along the a-axis. The anisotropy in the crystal and the DFT predicted electronic structure hinted at the anisotropic semiconducting property of the cluster crystals. This study has opened new opportunities to engineer ligands to create crystals of clusters with unidirectional conductivity.

All the work mentioned above are on the bulk properties of nanocluster assemblies or crystals. However, Feng et al. have recently reported the measurement of conductance of a single cluster using a MCBJ (mechanically controlled break junction) device.[73] In MCBJ, a skinny ductile metal wire is pulled to create a nanoscale gap contact of a single molecule, placed over a flexible base (shown in Figure 5e). The polymer base is then bent in a controlled manner so that the metal wire breaks and the contact is broken. After breaking, the gap between the two metal wires is adjusted to the separation distance equal to the cluster length, enabling the cluster to fit into this gap and create a contact between the broken metal wires. The electrical contact is made when there is an alignment of the molecular orbital of the cluster and the Fermi levels of the metal electrodes, and the change in potential when this contact is made is called the inflection point voltage or transition voltage (shown in Figure 5f).

Authors have studied the conductance of Ag_{25}, Ag_{43}, Ag_{44}, Ag_{63}, Ag_{78}, Ag_{141}, Ag_{136} and Ag_{374} clusters using MCBJ technique (shown in Figure 5d). The conductivity plots of all the clusters are shown in Figure 5g,

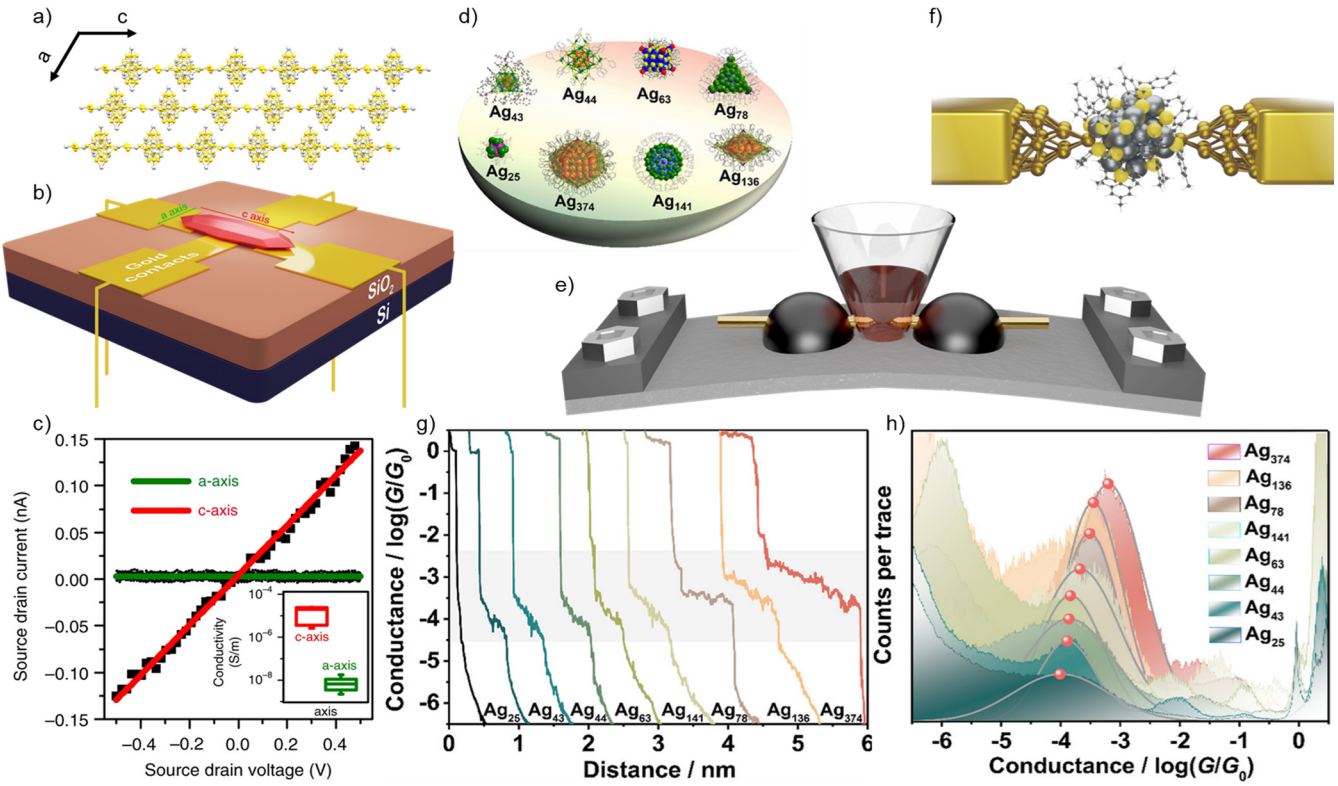

Figure 5: a) Intercluster packing of a bimetallic Au-Ag alloy cluster. **b)** Schematic representation of conductivity measurements of a single crystal of the same cluster. **c)** I-V plot of the crystal along different axial directions. **d)** Structural representation of various clusters involved for single particle conductivity measurements. **e)** Schematic representation of MCBJ device with a liquid cell. **f)** atomic dimension of gold electrodes holding a single cluster. **g)** Conductance traces of nanoclusters with different sizes as a function of distance between the gold electrodes. **h)** 1D conductance histograms of different nanocluster junctions. Reproduced with permission from Ref [72, 73]

h. The conductance in such small particles is through the tunneling of electrons through the molecule, which decreases with the increase in the length of the molecule according to the equation $G = Ae^{-\beta d}$, where G is conductance, A is the pre-exponential factor, β is tunneling decay constant and d is the length of the molecule. The β is size independent and depends on the tunneling barrier. Generally, the conductivity of clusters decreases exponentially with the increase in their length. However, the HOMO-LUMO gap decreases fairly rapidly with the increase in the size of clusters, and the β will become size-dependent. This arising dependency of β on the size of the cluster will likely eliminate the decay of conductance with the increasing size of the cluster. These results show that as the size of the cluster increases, the conductivity increases, which is contradictory to the observations made for other simple molecules. Normally tunneling of electrons through the vacuum requires a greater potential (> 1.0V) between electrodes separated by a distance. However, when a silver cluster occupies the junction, the potential for tunneling reduces to ~1.0V, which indicates a lower tunneling barrier for electrons through the clusters. It is also notable that the cluster metal core is involved in the conduction, not the ligand. This is evident because even though different ligands protect the silver clusters used here, the inflection point voltage for all the clusters is the same.

Conclusion and future perspective

This review summarizes the advancements in atomically precise clusters , especially for gold and silver, and the effect of confinement on their properties. The structural framework of such materials is presented in terms of their bonding and intermolecular interactions. We have discussed various types of the core structure of clusters and their subsequent expansion leading to the core-shell geometry of larger clusters. Surface ligands are essential in determining atomicity and for simultaneously determining clusters' physiochemical properties. Extended structural assembly of clusters in single crystals resulted in chirality, polymorphism, and framework solids, which has enabled us to understand more about such materials recently.

After the pioneering work of synthesizing colloidal gold nanoparticles in 1980 by Brust et al., extensive research over the last three decades witnessed significant progress in atomically precise materials. Many gold and silver nanoclusters with varying atomicity were synthesized and characterized through TEM, mass spectrometry, and other studies. Structural aspects of clusters were resolved through single crystal XRD, and electron diffraction and atom-specific chemical properties were correlated with structural aspects. Stability of ultrasmall particles is a primary concern for their practical applications. Use of bulky three-dimensional ligands (especially carborane thiols and alkynes) resulted in new clusters with better stability than their organic counterparts. Encapsulation using inorganic templates such as glass matrix, MOFs, and two-dimensional chalcogenides enables enhanced stability with composite properties. Other metal-based nanoclusters, especially Cu, Ni, Co, Pd, and Ru remain to be explored in detail due to their instability issues. The interaction of clusters with living organisms such as viruses and bacteria will be a new dimension to be explored. The species formed by the interaction of clusters and viruses can be studied using high-resolution megadalton mass spectrometry, which will provide information about the nature of interactions between these systems and will help us to implement clusters in medicine. Single particle conductivity and photoluminescence characteristics will open up new possibilities in ultrafast photoswitches, quantum computing, bioimaging, and other photonic applications. Machine learning and computer simulation of large clusters and their aggregates and crystals will help us understand their properties efficiently.

Acknowledgement

Authors acknowledge the support from Department of Science and Technology (DST), Govt. of India. T.P. acknowledges funding from the Centre of Excellence on Molecular Materials and Functions under the Institution of Eminence scheme of IIT Madras.

References

1. Jin, R.; Zeng, C.; Zhou, M.; Chen, Y. (2016). Atomically Precise Colloidal Metal Nanoclusters and Nanoparticles : Fundamentals and Opportunities. Chem. Rev. 116, 10346–10413.
2. Chakraborty, I.; Pradeep, T. (2017). Atomically Precise Clusters of Noble Metals : Emerging Link between Atoms and Nanoparticles. Chem. Rev. 117, 8208–8271.
3. Jena, P.; Sun, Q. (2018) Super Atomic Clusters : Design Rules and Potential for Building Blocks of Materials. Chem. Rev. 118, 5755–5870.
4. Udayabhaskararao, T.; Pradeep, T. (2013) New Protocols for the Synthesis of Stable Ag and Au Nanocluster Molecules. J. Phys. Chem. Lett. 4, 1553–1564.
5. Kang, X.; Zhu, M. (2019) Transformation of Atomically Precise Nanoclusters by Ligand-Exchange. Chem. Mater. 31 (24), 9939–9969.
6. Jana, A.; Chakraborty, P.; Dar, W. A.; Chandra, S.; Khatun, E.; Kannan, M. P.; Ras, R. H. A.; Pradeep, T. (2020) Dual Emitting Ag35 Nanocluster Protected by 2-Pyrene Imine Thiol. Chem. Commun. 56, 12550–12553.
7. Wang, Z. W.; Palmer, R. E. (2012) Experimental Evidence for Fluctuating, Chiral-Type Au55 Clusters by Direct Atomic Imaging. Nano Lett. 12 (11), 5510–5514.
8. Mahendranath, A.; Mondal, B.; Sugi, K. S.; Pradeep, T. (2022) Direct Imaging of Lattice Planes in Atomically Precise Noble Metal Cluster Crystals Using a Conventional Transmission Electron Microscope. Chem. Commun. 58 (12), 1906–1909.
9. AbdulHalim, L. G.; Bootharaju, M. S.; Tang, Q.; Del Gobbo, S.; AbdulHalim, R. G.; Eddaoudi, M.; Jiang, D. E.; Bakr, O. M. (2015) Ag29(BDT)12(TPP)4: A Tetravalent Nanocluster. J. Am. Chem. Soc. 137, 11970–11975.
10. Krishnadas, K. R.; Ghosh, A.; Baksi, A.; Chakraborty, I.; Natarajan, G.; Pradeep, T. (2016) Intercluster Reactions between Au25(SR)18 and Ag44(SR)30. J. Am. Chem. Soc. 138 (1), 140–148.
11. Krishnadas, K. R.; Baksi, A.; Ghosh, A.; Natarajan, G.; Pradeep, T. (2016) Structure-Conserving Spontaneous Transformations between Nanoparticles. Nat. Commun. 7, 1–9.
12. Krishnadas, K. R.; Baksi, A.; Ghosh, A.; Natarajan, G.; Som, A.; Pradeep, T. (2017) Interparticle Reactions: An Emerging Direction in Nanomaterials Chemistry. Acc. Chem. Res. 50 (8), 1988–1996.
13. Neumaier, M.; Baksi, A.; Weis, P.; Schneider, E. K.; Chakraborty, P.; Hahn, H.; Pradeep, T.; Kappes, M. M. (2021) Kinetics of Intercluster Reactions between Atomically Precise Noble Metal Clusters [Ag25(DMBT)18]- and [Au25(PET)18]- in Room Temperature Solutions. J. Am. Chem. Soc. 143 (18), 6969–6980.
14. Khatun, E.; Chakraborty, P.; Jacob, B. R.; Paramasivam, G.; Bodiuzzaman, M.; Dar, W. A.; Pradeep, T. (2020) Intercluster Reactions Resulting in Silver-Rich Trimetallic Nanoclusters. Chem. Mater. 32 (1), 611–619.
15. Chakraborty, P.; Nag, A.; Natarajan, G.; Bandyopadhyay, N.; Paramasivam, G.; Panwar, M. K.; Chakrabarti, J.; Pradeep, T. (2019) Rapid Isotopic Exchange in Nanoparticles. Sci. Adv. 5, 2–10.
16. Baksi, A.; Harvey, S. R.; Natarajan, G.; Wysocki, V. H.; Pradeep, T. (2016) Possible Isomers in Ligand Protected Ag11 Cluster Ions Identified by Ion Mobility Mass Spectrometry and Fragmented by Surface Induced Dissociation. Chem. Commun. 52 (19), 3805–3808.
17. Chakraborty, P.; Nag, A.; Paramasivam, G.; Natarajan, G.; Pradeep, T. (2018) Fullerene-Functionalized Monolayer-Protected Silver Clusters: [Ag29(BDT)12(C60)n]3- n= 1-9. ACS Nano 12, 2415–2425.
18. Nag, A.; Chakraborty, P.; Paramasivam, G.; Bodiuzzaman, M.; Natarajan, G.; Pradeep, T. (2018) Isomerism in Supramolecular Adducts of Atomically Precise Nanoparticles. J. Am. Chem. Soc. 140 (42), 13590–13593.
19. Jana, A.; Pradeep, T. (2023) Nanocluster assembled solids. Chapter 3, Elsevier, 49-82.
20. Antonello, S.; Dainese, T.; Pan, F.; Rissanen, K.; Maran, F. (2017) Electrocrystallization of Monolayer-Protected Gold Clusters: Opening the Door to Quality, Quantity, and New Structures. J. Am. Chem. Soc. 139, 4168–4174.
21. Jadzinsky, P. D.; Calero, G.; Ackerson, C. J.; Bushnell, D. A.; Kornberg, R. D. (2007) Structure of a Thiol Monolayer–Protected Gold Nanoparticle at 1.1 Å Resolution. Science 318, 430–434.
22. Azubel, M.; Koivisto, J.; Malola, S.; Bushnell, D.; Hura, G. L.; Koh, A. L.; Tsunoyama, H.; Tsukuda, T.; Pettersson, M.; Häkkinen, H.; Kornberg, R. D. (2014) Electron Microscopy of Gold Nanoparticles

at Atomic Resolution. Science 345 (6199), 909–912.
23. Liu, X.; Yan, H.; Chen, Y.; Yang, Y.; Porcar, L.; Radulescu, A.; Guldin, S.; Jin, R.; Stellacci, F.; Luo, Z. (2022) Quantifying the Solution Structure of Metal Nanoclusters Using Small-Angle Neutron Scattering. Angew. Chemie Int. Ed. 61, 1–7.
24. Wang, S.; Liu, T.; Jiang, D. E. (2021) Locating Hydrides in Ligand-Protected Copper Nanoclusters by Deep Learning. ACS Appl. Mater. Interfaces 13 (45), 53468–53474.
25. Shichibu, Y.; Negishi, Y.; Watanabe, T.; Chaki, N. K.; Kawaguchi, H.; Tsukuda, T. (2007) Biicosahedral Gold Clusters [Au25(PPh3)10(SCnH2n+1)5Cl2]2+ (n = 2-18): A Stepping Stone to Cluster-Assembled Materials. J. Phys. Chem. Lett. 111 (22), 7845–7847.
26. Jin, R.; Liu, C.; Zhao, S.; Das, A.; Xing, H.; Gayathri, C.; Xing, Y.; Rosi, N. L.; Gil, R. R.; Jin, R. (2015) Tri-Icosahedral Gold Nanocluster [Au37(PPh3)10(SC2H4Ph)10X2]+: Linear Assembly of Icosahedral Building Blocks. ACS Nano 9 (8), 8530–8536.
27. Yuan, S. F.; Xu, C. Q.; Liu, W. Di; Zhang, J. X.; Li, J.; Wang, Q. M. (2021) Rod-Shaped Silver Supercluster Unveiling Strong Electron Coupling between Substituent Icosahedral Units. J. Am. Chem. Soc. 143 (31), 12261–12267.
28. Song, Y.; Fu, F.; JunZhang; Chai, J.; Kang, X.; Li, P.; Li, S.; Zhou, H.; Zhu, M. (2015) The Magic Au60 Nanocluster: A New Cluster-Assembled Material with Five Au13 Building Blocks. Angew. Chemie - Int. Ed. 54, 8430–8434.
29. Malola, S.; Lehtovaara, L.; Knoppe, S.; Hu, K. J.; Palmer, R. E.; Bürgi, T.; Häkkinen, H. (2012) Au40(SR)24 Cluster as a Chiral Dimer of 8-Electron Superatoms: Structure and Optical Properties. J. Am. Chem. Soc. 134 (48), 19560–19563.
30. Malola, S.; Lehtovaara, L.; Häkkinen, H. (2014) A DFT Study of Linear Gold-Thiolate Superclusters Absorbing in the Therapeutic NIR Window. J. Phys. Chem. Lett. 5 (8), 1329–1334.
31. Du, X.; Chai, J.; Yang, S.; Li, Y.; Higaki, T.; Li, S.; Jin, R. (2019) Fusion Growth Patterns in Atomically Precise Metal Nanoclusters. Nanoscale 11 (41), 19158–19165.
32. Hu, F.; Guan, Z. J.; Yang, G.; Wang, J. Q.; Li, J. J.; Yuan, S. F.; Liang, G. J.; Wang, Q. M. (2021) Molecular Gold Nanocluster Au156 Showing Metallic Electron Dynamics. J. Am. Chem. Soc. 143 (41), 17059–17067.
33. Sakthivel, N. A.; Shabaninezhad, M.; Sementa, L.; Yoon, B.; Stener, M.; Whetten, R. L.; Ramakrishna, G.; Fortunelli, A.; Landman, U.; Dass, A. (2020) The Missing Link: Au191(SPh-TBu)66 Janus Nanoparticle with Molecular and Bulk-Metal-like Properties. J. Am. Chem. Soc. 142 (37), 15799–15814.
34. Zhou, M.; Zeng, C.; Song, Y.; Padelford, J. W.; Wang, G.; Sfeir, M. Y.; Higaki, T.; Jin, R. (2017) On the Non-Metallicity of 2.2 nm Au246(SR)80 Nanoclusters. Angew. Chemie - Int. Ed. 56 (51), 16257–16261.
35. Ma, M. X.; Ma, X. L.; Liang, G. M.; Shen, X. T.; Ni, Q. L.; Gui, L. C.; Wang, X. J.; Huang, S. Y.; Li, S. M. (2021) A Nanocluster [Ag307Cl62(SPhtBu)110]: Chloride Intercalation, Specific Electronic State, and Superstability. J. Am. Chem. Soc. 143, 13731–13737.
36. Zhou, Q.; Kaappa, S.; Malola, S.; Lu, H.; Guan, D.; Li, Y.; Wang, H.; Xie, Z.; Ma, Z.; Häkkinen, H.; Zheng, N.; Yang, X.; Zheng, L. (2018) Real-Space Imaging with Pattern Recognition of a Ligand-Protected Ag374 Nanocluster at Sub-Molecular Resolution. Nat. Commun. 9, 1–8.
37. Song, Y.; Lambright, K.; Zhou, M.; Kirschbaum, K.; Xiang, J.; Xia, A.; Zhu, M.; Jin, R. (2018) Large-Scale Synthesis, Crystal Structure, and Optical Properties of the Ag146Br2(SR)80 Nanocluster. ACS Nano 12, 9318–9325.
38. Chen, Y.; Zeng, C.; Kauffman, D. R.; Jin, R. (2015) Tuning the Magic Size of Atomically Precise Gold Nanoclusters via Isomeric Methylbenzenethiols. Nano Lett. 15 (5), 3603–3609.
39. Kang, X.; Chong, H.; Zhu, M. (2018) Au25(SR)18: The Captain of the Great Nanocluster Ship. Nanoscale 10 (23), 10758–10834.
40. Joshi, C. P.; Bootharaju, M. S.; Alhilaly, M. J.; Bakr, O. M. (2015) [Ag25(SR)18]-: The "Golden"Silver Nanoparticle Silver Nanoparticle. J. Am. Chem. Soc. 137 (36), 11578–11581.
41. Li, Y.; Zhou, M.; Song, Y.; Higaki, T.; Wang, H.; Jin, R. (2021) Double-Helical Assembly of Heterodimeric Nanoclusters into Supercrystals. Nature 594, 380–384.
42. Zhu, Y.; Guo, J.; Qiu, X.; Zhao, S.; Tang, Z. (2021) Optical Activity of Chiral Metal Nanoclusters. Accounts Mater. Res. 2 (1), 21–35.
43. Liang, X. Q.; Li, Y. Z.; Wang, Z.; Zhang, S. S.; Liu, Y. C.; Cao, Z. Z.; Feng, L.; Gao, Z. Y.; Xue, Q. W.; Tung, C. H.; Sun, D. (2021) Revealing the Chirality Origin and Homochirality Crystallization of Ag14 Nanocluster at the Molecular Level. Nat. Commun. 12 (1), 1–10.
44. Huang, J. H.; Wang, Z. Y.; Zang, S. Q.; Mak, T. C. W. (2020) Spontaneous Resolution of Chiral Multi-Thiolate-Protected Ag30 Nanoclusters. ACS Cent. Sci. 6 (11), 1971–1976.
45. Yoshida, H.; Ehara, M.; Priyakumar, U. D.; Kawai, T.; Nakashima, T. (2020) Enantioseparation and Chiral Induction in Ag29 Nanoclusters with Intrinsic Chirality. Chem. Sci. 11 (9), 2394–2400.
46. Jana, A.; Unnikrishnan, P. M.; Poonia, A. K.; Roy, J.; Jash, M.; Paramasivam, G.; Machacek, J.; Adarsh, K. N. V. D.; Base, T.; Pradeep, T. (2022) Carboranethiol-Protected Propeller-Shaped Photoresponsive Silver Nanomolecule. Inorg. Chem. 61 (23), 8593–8603.
47. Nag, A.; Chakraborty, P.; Bodiuzzaman, M.; Ahuja, T.; Antharjanam, S.; Pradeep, T. (2018) Polymorphism of Ag29(BDT)12(TPP)43- Cluster: Interactions of Secondary Ligands and Their Effect on Solid State Luminescence. Nanoscale 10 (21), 9851–9855.
48. Chen, Y.; Liu, C.; Tang, Q.; Zeng, C.; Higaki, T.; Das, A.; Jiang, D. (2016) Isomerism in Au28(SR)20 Nanocluster and Stable Structures. J. Am. Chem. Soc. 138, 1482–1485.
49. Bodiuzzaman, M.; Dar, W. A.; Pradeep, T. (2021) Cocrystals of Atomically Precise Noble Metal Nanoclusters. Small 17 (27), 1–15.
50. Yan, J.; Malola, S.; Hu, C.; Peng, J.; Dittrich, B.; Teo, B. K.; Häkkinen, H.; Zheng, L.; Zheng, N. (2018) Co-Crystallization of Atomically Precise Metal Nanoparticles Driven by Magic Atomic and Electronic Shells. Nat. Commun. 9 (1), 1–8.
51. Bodiuzzaman, M.; Ghosh, A.; Sugi, K. S.; Nag, A.; Khatun, E. (2019) Camouflaging Structural Diversity : Co-Crystallization of Two Different Nanoparticles Having Different Cores but the Same Shell. Angew. Chemie - Int. Ed. 58, 189–194.
52. Dar, W. A.; Bodiuzzaman, M.; Ghosh, D.; Paramasivam, G.; Khatun, E.; Sugi, K. S.; Pradeep, T. (2019) Interparticle Reactions between Silver Nanoclusters Leading to Product Cocrystals by Selective Cocrystallization. ACS Nano 13, 13365–13373.
53. Kang, X.; Zhu, M. (2020) Cocrystallization of Atomically Precise Nanoclusters. ACS Mater. Lett. 2 (10), 1303–1314.
54. Liu, J. Y.; Alkan, F.; Wang, Z.; Zhang, Z. Y.; Kurmoo, M.; Yan, Z.; Zhao, Q. Q.; Aikens, C. M.; Tung, C. H.; Sun, D. (2019) Different Silver Nanoparticles in One Crystal: Ag210(iPrPhS)71(Ph3P)5Cl and Ag211(iPrPhS)71(Ph3P)6Cl. Angew. Chemie - Int. Ed. 58, 195–199.
55. Huang, R. W.; Wei, Y. S.; Dong, X. Y.; Wu, X. H.; Du, C. X.; Zang, S. Q.; Mak, T. C. W. (2017) Hypersensitive Dual-Function Luminescence Switching of a Silver-Chalcogenolate Cluster-Based Metal-Organic Framework. Nat. Chem. 9 (7), 689–697.
56. Wang, Z.; Wang, M.; Li, Y.; Luo, P.; Jia, T.; Huang, R.; Zang, S.; Mak, T. C. W. (2018) Atomically Precise Site-Specific Tailoring and Directional Assembly of Superatomic Silver Nanoclusters. J. Am. Chem. Soc. 140, 1069–1076.
57. Dar, W. A.; Jana, A.; Sugi, K. S.; Paramasivam, G.; Bodiuzzaman, M.; Khatun, E.; Som, A.; Mahendranath, A.; Chakraborty, A.; Pradeep, T. (2022) Molecular Engineering of Atomically Precise Silver Clusters into 2D and 3D Framework Solids. Chem. Mater. 34 (10), 4703–4711.
58. Wang, Y. M.; Zhang, J. W.; Wang, Q. Y.; Li, H. Y.; Dong, X. Y.; Wang, S.; Zang, S. Q. (2019) Fabrication of Silver Chalcogenolate Cluster Hybrid Membranes with Enhanced Structural Stability and Luminescence Efficiency. Chem. Commun. 55 (97), 14677–14680.
59. Kang, X.; Zhu, M. (2019) Tailoring the Photoluminescence of Atomically Precise Nanoclusters. Chem. Soc. Rev. 48, 2422–2457.
60. Chen, Y.; Zhou, M.; Li, Q.; Gronlund, H.; Jin, R. (2020) Isomerization-Induced Enhancement of Luminescence in Au28(SR)20 nanoclusters. Chem. Sci. 11, 8176–8183.
61. Goswami, N.; Yao, Q.; Luo, Z.; Li, J.; Chen, T.; Xie, J. (2016) Luminescent Metal Nanoclusters with Aggregation-Induced Emission. J. Phys. Chem. Lett. 7, 962–975.
62. Kang, X.; Wang, S.; Zhu, M. (2018) Observation of a New Type of Aggregation-Induced Emission in Nanoclusters. Chem. Sci. 9, 3062–3068.
63. Khatun, E.; Ghosh, A.; Chakraborty, P.; Singh, P.; Bodiuzzaman, M.; Ganesan, P.; Nataranjan, G.; Ghosh, J.; Pal, S. K.; Pradeep, T. (2018) A Thirty-Fold Photoluminescence Enhancement Induced by Secondary Ligands in Monolayer Protected Silver Clusters. Nanoscale 10 (42), 20033–20042.
64. Chen, T.; Yang, S.; Chai, J.; Song, Y.; Fan, J.; Rao, B.; Sheng, H.; Yu, H.; Zhu, M. (2017) Crystallization-Induced Emission Enhancement: A Novel Fluorescent Au-Ag Bimetallic Nanocluster with Precise Atomic Structure. Sci. Adv. 3, 1–8.
65. Khatun, E.; Bodiuzzaman, M.; Sugi, K. S.; Chakraborty, P.; Paramasivam, G.; Dar, W. A.; Ahuja, T.; Antharjanam, S.; Pradeep, T. (2019) Confining an Ag10 Core in an Ag12 Shell: A Four-Electron Superatom with Enhanced Photoluminescence upon Crystallization. ACS Nano 13 (5), 5753–5759.
66. Jana, A.; Jash, M.; Poonia, A. K.; Paramasivam, G.; Islam, M. R.; Chakraborty, P.; Antharjanam, S.; Machacek, J.; Ghosh, S.; Adarsh, K. N. V. D.; Base, T.; Pradeep, T. (2021) Light-Activated Intercluster Conversion of an Atomically Precise Silver Nanocluster. ACS Nano 15 (10), 15781–15793.
67. Wang, Z.; Su, H.; Tan, Y.; Schein, S.; Lin, S.; Liu, W.; Wang, S.; Wang, W.; Tung, C.; Sun, D.; Zheng, L. (2017) Assembly of Silver Trigons into a Buckyball-like Ag180 Nanocage. Proc. Natl. Acad. Sci. U. S. A. 114(46), 12132–12137.
68. Li, Q.; Mosquera, M. A.; Jones, L. O.; Parakh, A.; Chai, J.; Jin, R.; Schatz, G. C.; Gu, X. W. (2020) Pressure-Induced Optical Transitions in Metal Nanoclusters. ACS Nano 14, 11888–11896.
69. Sun, Q.-Q.; Li, Q.; Li, H.-Y.; Zhang, M.-M.; Sun, M.-E.; Li, S.; Quan, Z.; Zang, S.-Q. (2021) Thermochromism and Piezochromism of an Atomically Precise High-Nuclearity Silver Sulfide Nanocluster. Chem. Commun. 57, 2372–2375.
70. Wang, Z.; Su, H. F.; Gong, Y. W.; Qu, Q. P.; Bi, Y. F.; Tung, C. H.; Sun, D.; Zheng, L. S. (2020) A Hierarchically Assembled 88-Nuclei Silver-Thiacalix[4]Arene Nanocluster. Nat. Commun. 11, 1–8.
71. Li, Q.; Russell, J. C.; Luo, T. Y.; Roy, X.; Rosi, N. L.; Zhu, Y.; Jin, R. (2018) Modulating the Hierarchical Fibrous Assembly of Au Nanoparticles with Atomic Precision. Nat. Commun. 9, 1–7.
72. Yuan, P.; Zhang, R.; Selenius, E.; Ruan, P.; Yao, Y.; Zhou, Y.; Malola, S.; Häkkinen, H.; Teo, B. K.; Cao, Y.; Zheng, N. (2020). Solvent-Mediated Assembly of Atom-Precise Gold–Silver Nanoclusters to Semiconducting One-Dimensional Materials. Nat. Commun. 11, 1–8.
73. Feng, A.; Hou, S.; Yan, J.; Wu, Q.; Tang, Y.; Yang, Y.; Shi, J.; Xiao, Z.; Lambert, C. J.; Zheng, N.; Hong, W. (2022). Conductance Growth of Single-Cluster Junctions with Increasing Sizes. J. Am. Chem. Soc. 144 (34), 15680–15688.